Photochemical & Photobiological Sciences

ROYAL SOCIETY OF CHEMISTRY

TECHNICAL NOTE

Cite this: *Photochem. Photobiol. Sci.*, 2020, **19**, 1470

Microcystis aeruginosa inactivation and microcystin-LR degradation by the photo-Fenton process at the initial near-neutral pH

Mariana de Almeida Torres, *[a] Joicy Micheletto,[b] Marcus Vinicius de Liz,[c] Thomaz Aurélio Pagioro,[c] Lucia Regina Rocha Martins[c] and Adriane Martins de Freitas [c]

Received 5th May 2020,
Accepted 7th August 2020

DOI: 10.1039/d0pp00177e

rsc.li/pps

Of all cyanobacteria, *Microcystis aeruginosa* is the most commonly found species in bloom episodes all over the world. This species is known to produce cyanopeptides with hepatotoxic effects, namely microcystins (MCs). In this regard, Advanced Oxidation Processes (AOPs) have been widely studied for cyanotoxin degradation, but very few studies focused on cyanobacteria inactivation combined with toxin removal. To our knowledge, this is the first report of the photo-Fenton process application focusing on *M. aeruginosa* inactivation and microcystin-LR (MC-LR) degradation. This research work aimed to evaluate the photo-Fenton process under three different conditions with regard to Fe^{2+}/H_2O_2 ratios (0.6/10, 5/50, and 20/100 mg L^{-1}) at the initial near-neutral pH. Process efficiency was measured by immediate cell density reduction, growth inhibition, effect on MC-LR concentrations, and scanning electron microscopy (SEM) to analyze any alterations in cell morphology. Growth inhibition test (GIT) results pointed to cell inactivation under all conditions tested, and MC-LR concentrations were reduced below WHO's maximum limit at medium and higher concentrations of reagents. The possible mechanisms of cell inactivation by oxidative species are discussed.

1. Introduction

Cyanobacteria are photosynthetic prokaryotic organisms that form a large and diverse group, and they are capable of living in different environments. However, most species show optimum growth in freshwater environments, with neutral to alkaline pH and higher temperatures, making aquatic ecosystems the habitats of their greatest occurrence.[1]

In some cases, depending on the environmental conditions (such as high nutrient input caused by untreated wastewater discharge or use of fertilizers), accelerated growth of these organisms is observed, making them the dominant part of phytoplankton in lakes, reservoirs, and rivers. These episodes are known as cyanobacterial blooms.[2] Recent evidence has shown that bloom events are increasing in duration, magnitude, and frequency all over the world, and this might be associated with climate change.[2,3]

The main concern associated with high densities of cyanobacteria in aquatic environments is related to the ability of these organisms to synthesize potentially toxic metabolites (known as cyanotoxins).[4,5]

Of all cyanobacteria reported from around the world, *Microcystis aeruginosa* is the most notorious species in bloom episodes.[6] This species and other cyanobacterial species are capable of producing toxins with known hepatotoxic effects (microcystins), which are the most widespread. Microcystins (MCs) are cyclic heptapeptides with the characteristic Adda moiety (3-amino-9-methoxy-2,6,8-trimethyl-10-phenyl-deca-4,6-dienoic acid) and two variable amino acids in positions (2) and (4). More than 200 MC variants have been identified so far, and microcystin-LR (variant with leucine (L) and arginine (R)) is known to be the most toxic and frequently found.[7] Due to its risks, the World Health Organization (WHO) proposed 1 μg L^{-1} as the limit for microcystins in drinking and recreational water.[8]

The presence of cyanobacteria in water reservoirs represents a serious problem to water treatment plants since not all treatments are able to reduce cyanotoxin levels in accordance with the current legislation.[9] The literature reports the efficiency of several treatments in cyanotoxin removal, such as activated carbon, chlorination, coagulation, sedimentation and flotation

[a]*Postgraduate Program in Pathophysiology and Toxicology – School of Pharmaceutical Sciences, University of São Paulo, São Paulo, Brazil. E-mail: marianatorres@usp.br*
[b]*Geology Department, Federal University of Paraná, Curitiba, Brazil*
[c]*Department of Chemistry and Biology, Federal University of Technology – Parana, Curitiba, Brazil*

(removing intracellular toxins), membrane filtration, oxidation methods, and Advanced Oxidation Processes (AOPs – such as TiO_2 photocatalysis, UV/H_2O_2, and sulfate radical-based AOPs).[10–12] Amongst the AOPs, the photo-Fenton process has been largely explored for cyanotoxin degradation. This well-known light-assisted reaction between hydrogen peroxide (H_2O_2) and ferrous iron (Fe^{2+}) is characterized by the formation of hydroxyl radicals, which are powerful oxidants as they are non-selective and highly reactive. This reaction is usually carried out at acidic pH; however, in the past decade, several studies have shown its efficiency at circumneutral pH.[13]

Few studies have reported cyanobacteria inactivation with simultaneous cyanotoxin removal by AOPs and other novel techniques,[14–19] including the sono-Fenton hybrid process.[20] However, there are no reports specifically about photo-Fenton oxidation. There are, however, some studies that have reported the ability of the photo-Fenton process (at near-neutral pH) in inactivating pathogenic microorganisms, such as bacteria, protozoa and fungi spores.[21–27]

Considering this background, the present study evaluates the potential of the circumneutral photo-Fenton process in *Microcystis aeruginosa* inactivation and degradation of intra- and extracellular microcystin-LR in aqueous medium, by testing three different Fe^{2+}/H_2O_2 ratios.

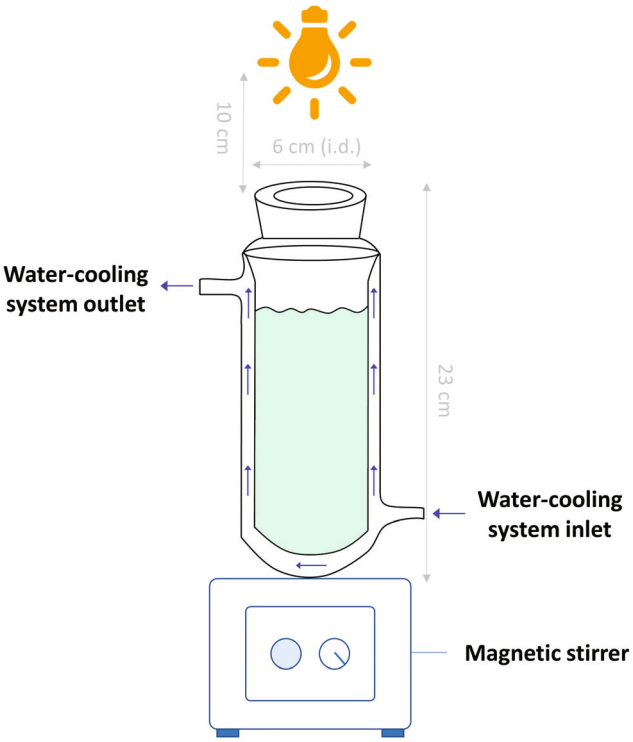

Fig. 1 Schematic representation of the reactor.

2. Materials and methods

2.1 Chemicals

All solvents were HPLC grade and high-purity water was obtained from a Mega Purity® system (Millipore Corporation, USA). Hydrogen peroxide (35%) was obtained from Peróxidos do Brasil Ltda. and ferrous sulfate from Vetec Química Fina Ltda. Bovine catalase (0.1 g L^{-1}, Sigma-Aldrich) was used to decompose residual H_2O_2 and subsequently interrupt the Fenton reaction. Other reagents were analytical grade.

2.2 *Microcystis aeruginosa* culture

The *Microcystis aeruginosa* strain (code BB005) isolated from a harmful bloom in the Barra Bonita reservoir (São Paulo, Brazil) was provided by the Botany department of the Federal University of São Carlos, Brazil. Cells were cultured in flasks containing ASM-1 medium[28] with an initial cell density inoculum of 1.6×10^5 cells per mL and maintained as follows: 25 ± 3 °C, luminosity of 2150 ± 230 lux and 12 : 12 (light : dark) photoperiod.

2.3 Experimental setup

Photo-Fenton experiments were carried out in a photochemical reactor (500 mL capacity, internal diameter: 6 cm, external diameter: 7.5 cm, total height: 23 cm) (Fig. 1), with a magnetic stirrer and a water-cooling system (to avoid thermal inactivation). The radiation was provided by a high-pressure mercury lamp (125 W, Osram) in which the original bulb had been replaced by a Pyrex glass bulb. The ultraviolet radiation intensity (UV-A) was 22.3 mW cm^{-2}, measured with a UV-A Instrutherm MRUR 202 radiometer. The equivalent intensity corresponding to the visible spectrum (425–700 nm) was 1.08×10^5 lux (measured with a digital luxmeter Minipa MLM-1011), and the lamp was maintained horizontally 10 cm above the reactor. Using the conversion factor of 0.011 suggested by Sylvania/Osram (the lamp manufacturer), this measure corresponds to approximately 1188 micromole photons per m^2 per s.[29] This experimental setup has also been described in a previous study.[30]

Cells in the exponential growth phase (1.5×10^6 cells per mL) were directly suspended in modified ASM-1 medium (with lower concentrations of nitrate and phosphate) to simulate a natural aquatic environment. The initial cell density and pH were 1×10^5 cells per mL and 6.8 ± 0.2 (respectively) in all experiments, and the initial treatment volume was 500 mL.

M. aeruginosa inactivation by the photo-Fenton process at circumneutral pH was evaluated at three different initial ratios between hydrogen peroxide and iron (Fe^{2+}/H_2O_2): 0.6/10 (I), 5/50 (II) and 20/100 (III) mg L^{-1}, and these experiments were carried out in triplicate. As there were no reports of similar processes being studied with cyanobacterial cells, the concentrations were based on studies in which the photo-Fenton process had been applied with neutral pH in bacteria, which are structurally similar to cyanobacteria. The H_2O_2 and Fe^{2+} concentrations for I and III were established according to previous studies with *Escherichia coli*[24] (for the milder condition) and enteric bacterial cells[31] (for the highest concentrations). Condition II was chosen considering an intermediate ratio between I and III.

Three aliquots (17 mL) were taken during treatment (0, 45 and 90 minutes) to analyze the immediate cell density, growth inhibition, and hydrogen peroxide and dissolved iron concentrations. Temperature, pH and light intensity were monitored continuously throughout the treatment. MC-LR levels were also analyzed before and after treatment.

Control experiments (effects of mechanical stress, pH and radiation) were also performed with the same setup as mentioned above.

2.4 Cell counting and scanning electron microscopy (SEM) analysis

Cell density was determined by cell counting using a Neubauer chamber and microscopic analyses (Leica®, 400× amplification).

The effect of the photo-Fenton process on cellular morphology was evaluated using scanning electron microscopy (SEM). Cyanobacterial samples were first centrifuged at 8000 rpm (10 °C), the supernatant was discarded, and the pellet was fixed with 3% glutaraldehyde. After that, 10 μL of the sample was glued on slides and subsequently dehydrated in 25, 50, 70, and 100% ethanol solutions (three times, 10 min for each stage). The dried samples were sputter-coated with gold and then observed and photographed with an SEM microscope (Zeiss, EVO MA15).

2.5 Growth inhibition tests (GIT)

Growth inhibition tests (GIT) were carried out in test tubes. Under sterile conditions, aliquots (2 mL) from the reactor were inoculated in 18 mL of ASM-1 medium, and growth was measured by cell counting after a 15-day incubation period (carried out as mentioned in section 2.3). The non-exposed culture was used as a control, and all growth experiments were carried out in triplicate.

2.6 Analytical determinations

Hydrogen peroxide was analyzed by a colorimetric method (395 nm) using titanium salt at acidic pH.[32] The iron concentration was determined according to the *o*-phenanthroline standardized procedure (510 nm).[33]

For MC-LR analyses, aliquots of treated and non-treated samples were subjected to three freeze–thaw cycles (for cell disruption), filtered with nylon membranes (0.45 μm porosity) and extracted using C18 cartridges (Applied Separations) that were pre-conditioned with 10 mL of methanol and 10 mL of ultrapure water, followed by 100 mL of the sample. The analytes were desorbed with 10 mL of MeOH, which was evaporated to dryness in an air flush system and redissolved in 500 μL of ultrapure water.

MC-LR analyses were performed by liquid chromatography (Prominence®, Shimadzu) with a diode array detector. The chromatographic method was conducted using a C18 polymeric analytical column (X-Terra®, Waters; 150 × 30 mm i.d., 3.5 μm particle size) coupled with a C18 guard column (Phenomenex). The mobile phase consisted of an aqueous solution of trifluoroacetic acid 0.05% v/v (solvent A) and methanol (solvent B) in an isocratic elution (50%) for 50 minutes, followed by a linear gradient (55 to 100% of B in 2 minutes, 100% of B for 20 minutes and return to the initial condition in 2 minutes). The flow rate was 0.3 mL min^{-1} and the column temperature was set at 35 °C. The LC method was validated based on the Bioanalytical Method Validation M10 guideline from ICH (International Conference on Harmonization)[34] using appropriate dilutions of the MC-LR analytical standard (Enzo Life Sciences, ≥95% purity). Linearity was verified with external calibration and by standard addition (0.03; 0.3; 0.6; 0.9; 1.2 and 1.5 mg L^{-1}), and intermediary precision and accuracy (recovery analyses) were evaluated by quality control levels at low (0.1 mg L^{-1}), medium (0.7 mg L^{-1}) and high (1.3 mg L^{-1}) concentrations with regard to the calibration curve ($y = 322.481 \pm 2.637x - 3283.2 \pm 2396$; $R^2 = 0.09998$). The limit of detection was 22 μg MC-LR per L, calculated by three times the standard deviation of the intercept (b) of three calibration curves (triplicates), divided by the slope of the equation (a) (LOD = (SD of $b \times 3$)/a); the lower limit of quantification was 30 μg MC-LR per L. Therefore, it was possible to quantify concentrations above 0.15 μg L^{-1}, considering the sample concentration factor of 200 times.

2.7 Calculations and statistics

Mean, standard deviation, graphical and statistical analyses were performed using the Microsoft® Excel 2020 software. Logarithmic trend lines in the plots, representing 3 independent experiment averages, were also calculated using Microsoft® Excel.

Differences in immediate cell counting and the GIT results during the treatment were assessed by an independent sample *t*-test. A probability level of $p \leq 0.05$ was used to reject the null hypothesis that there was no effect of the photo-Fenton treatment on the immediate cell density and growth inhibition.

3. Results and discussion

3.1 Photo-Fenton treatment

The photo-Fenton process at the lowest ratio (condition I) showed approximately 40% cell density reduction after 90 minutes of treatment (Fig. 2a). Under this condition, the GIT pointed to a complete loss of cell viability within 45 minutes (Table 1). H_2O_2 concentrations were reduced by 24%, and total dissolved iron concentrations indicated that only 0.37 mg L^{-1} from the 0.6 mg L^{-1} added was dissolved immediately at the beginning of the reaction, with Fe^{3+} being the most abundant (Fig. 2a). The pH was maintained stable (6.12 ± 0.11) after iron addition and after 45 minutes of the reaction, only Fe^{3+} could be quantified. Under this condition, total MC-LR concentrations reduced from 3.58 μg L^{-1} to 2.74 μg L^{-1}, representing 24% reduction. However, these levels were not below the maximum limit established by the WHO (1 μg L^{-1}).

When the process was tested with condition II, the cell density was reduced by 51% (Fig. 2b), and the GIT also

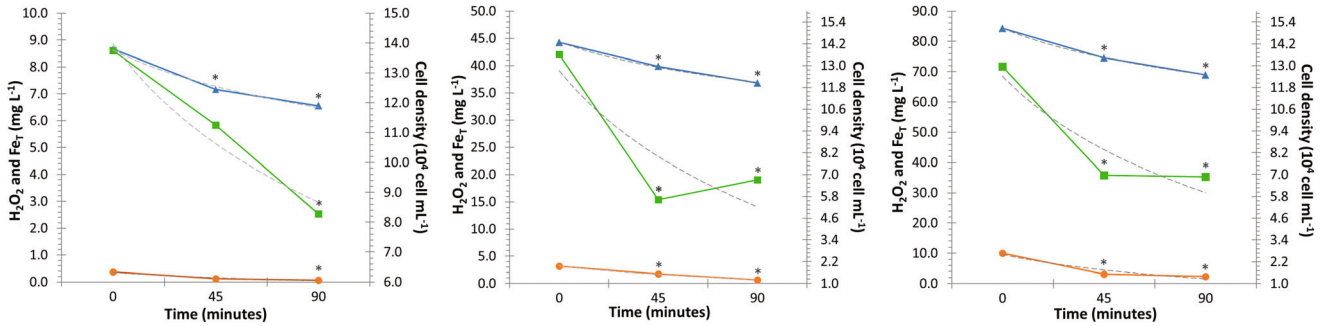

Fig. 2 Hydrogen peroxide (▲), total dissolved iron (●) and cell density (■) during the photo-Fenton process under conditions I (a), II (b) and III (c); (– – –) indicates logarithmic trend lines in the plots representing 3 independent experiment averages; asterisks indicate statistically significant differences between the treated and control samples (*t*-test, $p < 0.05$).

Table 1 Growth inhibition test (GIT) results after photo-Fenton treatment at three different Fe^{2+}/H_2O_2 ratios

Iron–H_2O_2 concentrations (mg L^{-1})	0.6–10			5–50			20–100		
Time	0 min	45 min	90 min	0 min	45 min	90 min	0 min	45 min	90 min
GIT (10^6 cells per mL)	2.30 ± 0.07	<DL	<DL	2.25 ± 0.12	<DL	<DL	1.26 ± 0.10	<DL	<DL

<DL: Values below the detection limit (1×10^4 cells per mL); $N = 3$; data of the GIT are presented as mean ± SD.

suggested a loss of cell viability within 45 minutes (Table 1). Iron analysis indicated that early in the reaction the total iron concentration was 3.21 mg L^{-1} (being 1.70 mg L^{-1} of Fe^{2+} and 1.51 mg L^{-1} of Fe^{3+}), but at the end, the iron concentration decreased by 79% (Fig. 2b). After iron addition, the pH dropped to 3.75 ± 0.02. Under these conditions, hydrogen peroxide consumption was about 17% (from 44.28 to 36.82 mg L^{-1}) and MC-LR concentrations were below the detection limit after 90 minutes of treatment for all replicates, suggesting high degradation of the toxin.

The photo-Fenton treatment in the highest Fe^{2+}/H_2O_2 ratio (condition III) pointed to 47% cell density reduction (Fig. 2c) and, similar to the other experiments, no growth was observed in the GIT after 45 minutes (Table 1). Hydrogen peroxide was reduced by 18%, and total iron concentrations were reduced by 88% (Fig. 2c), and only ferric forms were dissolved (90 minutes) (pH 3.15 ± 0.07). Total MC-LR analysis pointed to 78% reduction (3.58 μg L^{-1} to 0.80 μg L^{-1}, below WHO's maximum concentration limit) in only one replica, and the other replicates presented concentrations below the detection limit.

Under conditions II and III (where the iron concentrations were higher), the pH dropped significantly. At the initial near-neutral pH, iron precipitates as iron hydroxides, which is the predominant species. Fe^{3+} may form oxides and precipitate on existing oxides, and this precipitation dislocates the chemical balance causing a sharp decrease in the pH.[35]

Sun and co-workers[17] found that the UV/chlorine process was able to degrade intra- and extracellular MC-LR and affect the regrowth of the cells after a 10-day incubation period with chlorine dosages above 1 mg L^{-1}.

Within 90 minutes of the reaction (in all three cases), dissolved ferric forms predominated, but the cell density was still reduced. These results suggest the occurrence of alternative pathways and secondary reactions of the formed oxidative species, such as the Fenton-like process.[24]

When the photo-Fenton process was studied with higher concentrations of iron species (conditions II and III), the formation of cell aggregates was observed, similar to the mucilaginous sheath seen in strains of *Microcystis aeruginosa*. However, the strain used for these experiments did not form aggregates during culture or before the experiments. These effects might be related to the Fe^{3+} capacity to bind with negatively charged cell surfaces. Spuhler *et al.* (2010)[24] reported adsorption of Fe^{3+} on the *Escherichia coli* cell wall forming Fe^{3+}–bacteria complexes. According to the authors, cell walls have highly reactive surfaces with outer membrane-binding proteins, other proteins, and carboxylic groups, capable of bonding with iron.

The overall inactivation method described in the literature is related to the oxidative species formed during the photo-Fenton process, notably hydroxyl radicals. These radicals attack the external cell membrane, initiating lipid peroxidation chain reactions and increasing its permeability.[15,27]

The photo-Fenton process did not entirely reduce the cell density, but MC-LR decreased sharply when Fe^{2+} and H_2O_2 were under conditions II and III. These results suggest the degradation of the toxin at an intracellular level. H_2O_2 and reactive oxygen species (ROS) can permeate the cell and elevate membrane permeability, facilitating Fe^{2+} diffusion into the cell and Fe^{3+} adsorption in cell walls. Many authors have suggested the probability of intracellular oxidation (*e.g.*, Fenton reaction) once Fe^{2+} catalyzed ROS formation.[20,22,26,27] These reactive species generated inside or diffused into the cell can degrade intracellular metabolites (such as MCs) and damage lipids,

pigments, other proteins (enzymes), and DNA,[26,27] explaining the cell inactivation and toxin degradation.

While these oxidative species are capable of degrading intracellular components, oxides and ferric-organic complexes formed during the reaction demonstrate that another possible contribution for the cell removal (and consequently reduction of MC-LR concentrations) is *via* precipitation. This explanation was also proposed by Jia *et al.* (2018),[19] who showed the reduction of algal and total organic matter after UVC/H_2O_2 pre-oxidation and iron precipitation.

Through transcriptomic analysis, Wang *et al.* (2018)[36] found that the photosynthesis- and MC biosynthesis-related genes (mcyA and mcyD) were downregulated after H_2O_2 exposure, and CYPs mediated the effects on photosynthesis, synthesis and release of MCs of *M. aeruginosa* at the gene level. These mechanisms can also be inferred to be responsible for cell inactivation (considering the hydrogen peroxide exposure).

The intensive radiation used in the photo-Fenton process can also increase the formation of oxidative species, and exposure of photosynthetic organisms to intense light can also result in PSII inactivation. When the radiation intensity is higher than the capacity of the photosynthetic electron flow, $^1O_2$ production can increase, and other ROS can be formed, leading to the inactivation of photosystems.[37]

This explains why low consumption of H_2O_2 does not imply that the inactivation process had stopped once delayed effects began to occur, including transcriptional responses caused by accumulated DNA mutations provoked by intracellular ROS formed due to UVA radiation.[26,38] Also, it is important to mention the synergic effects of H_2O_2 with radiation, which can generate ROS by its homolytic cleavage and damage cells.[18] In addition, enzymes responsible for the elimination of oxidative species (such as catalase and sodium dismutase), when exposed to UV-A light, can be inactivated and increase ROS concentrations in the cell.[24,26] Fig. 3 presents the possible inactivation mechanisms of *M. aeruginosa* when subjected to the photo-Fenton process.

3.2 Effect of longer reaction time on MC-LR concentrations at lower concentrations of Fe^{2+} and H_2O_2

The photo-Fenton process was carried out for 240 minutes, and the cell density was reduced by 55% during the reaction (Table 2). Cell viability was entirely lost within 45 minutes. The hydrogen peroxide concentration decreased by 33%, and at

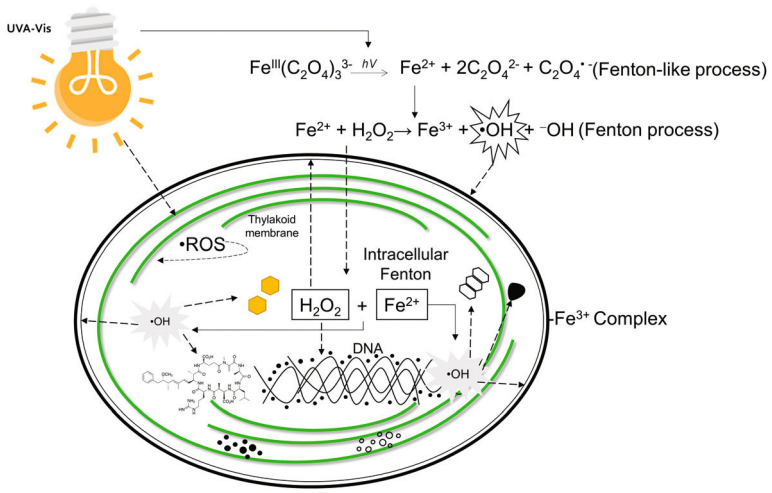

Fig. 3 Schematic representation of the possible pathways of *Microcystis aeruginosa* inactivation during the photo-Fenton process.

Table 2 Cell density, GIT, H_2O_2, Fe and MC-LR results after 240 minutes of photo-Fenton treatment in *M. aeruginosa* cells (condition I)

Parameter	0 min	45 min	90 min	180 min	240 min
pH	5.8	5.4	5.8	5.8	5.7
Temperature (°C)	25	25	25	25	26
Cell density (10^5 cells per mL)	1.40 ± 0.32	1.23 ± 0.17	0.72 ± 0.18*	1.15 ± 0.29	0.62 ± 0.50*
H_2O_2 (mg L^{-1})	10.11	8.38	7.71	6.46	6.80
Fe_T (mg L^{-1})	0.47	0.15	0.47	0.17	<DL
Fe^{2+} (mg L^{-1})	0.21	<DL	0.29	<DL	<DL
GIT (10^6 cells per mL)	2.08 ± 0.11	<DL	<DL	<DL	<DL
MC-LR (μg L^{-1})	3.96	3.64	2.34	2.83	2.64

Data of the immediate cell density and the GIT are represented as mean ± SD, and asterisks indicate statistically significant differences between the treated and control samples (*t*-test, $p < 0.05$); <DL: values below the detection limit (1×10^4 cells per mL).

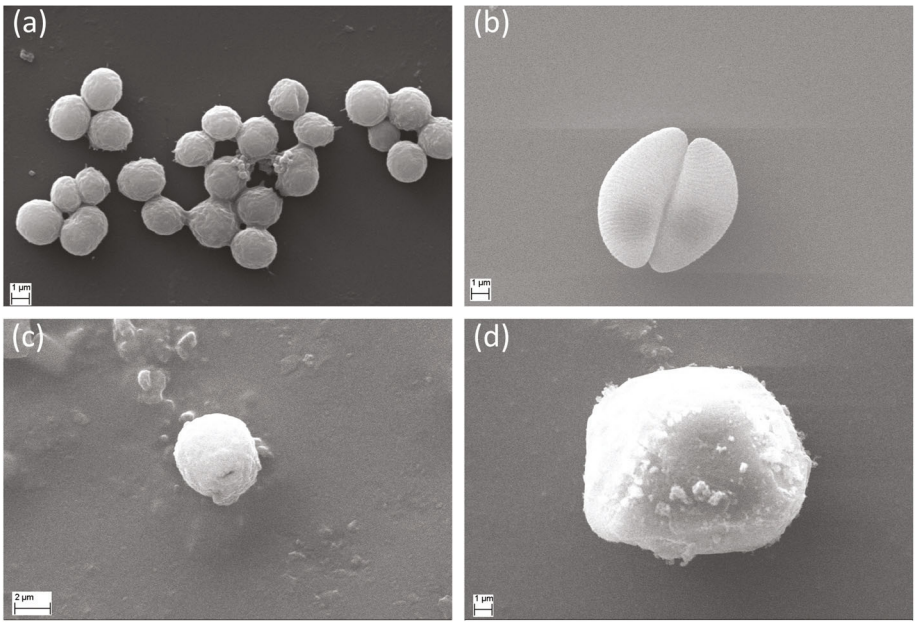

Fig. 4 Scanning electron micrographs of *Microcystis aeruginosa* cells before (a and b) and after (c and d) 240 minutes of the photo-Fenton process.

Table 3 Temperature, pH, cell density and growth inhibition test (GIT) results of the isolated effect analysis of radiation, pH and mechanical stress

	Radiation		Acidic pH		Mechanical stress	
Parameter	0 min	90 min	0 min	90 min	0 min	90 min
pH	6.5	6.3	3.7	3.9	6.8	6.8
Temperature (°C)	24	23	25	26	24	25
Cell density (10^5 cells per mL)	1.43 ± 0.21	1.32 ± 0.18	1.63 ± 0.43	1.41 ± 0.15	0.84 ± 0.09	0.82 ± 0.10
GIT (10^5 cells per mL)	6.70 ± 2.12	2.96 ± 0.61	5.60 ± 0.28	3.36 ± 0.04	17.8 ± 0.12	25.1 ± 0.06

Data of the immediate cell density and the GIT are represented as mean ± SD, and there were no statistically significant differences between the treated and control samples (*t*-test, $p < 0.05$).

240 minutes, ferric and ferrous iron concentrations dropped below the detection limit. MC-LR concentrations reduced from 3.96 to 2.64 μg L^{-1} (33%).

It must be noted that Fe^{2+} concentrations dropped until the detection limit within 45 minutes but increased in 90 minutes (0.29 mg L^{-1}). Soares *et al.* (2015)[39] observed a similar effect on iron concentrations and explained that it is related to the formation of ferric-organic complexes with the dissolved organic matter (in our case, originated during the oxidation of the cells). After they are formed, the reaction rate rises with the increase of dissolved iron concentrations and consumption of H_2O_2, indicating that these ferric-organic complexes were degraded, and iron species were redissolved.

Once the cells were inactivated, but the cell density was not entirely diminished, SEM analyses were performed to confirm the damage or morphological changes. The cellular aspect after the oxidative process indicated some differences when compared to fresh cultivated cells (Fig. 4a and b), such as irregular shapes, cell wall wrinkling, and rough cell surface of the treated cells as compared to healthy ones (Fig. 4c and d).

3.3 Isolated effects of pH, mechanical stress and radiation

Since photo-Fenton experiments in *Microcystis aeruginosa* pointed to complete inactivation of the cells, possible mechanical stress (promoted by magnetic stirring), light and acidic pH were experimentally investigated in an attempt to discover if these results could be attributed to the treatment itself or one of these system components alone. The pH was chosen considering the lowest value obtained after ferrous sulfate addition at the highest concentration of Fe^{2+} (20 mg L^{-1}) in the photo-Fenton process. The experimental setup was the same as used in the photo-Fenton experiments. The results (Table 3) did not show a statistical difference in cell density or growth inhibition before and after 90 minutes of exposure to light, acidic pH, or magnetic stirring, indicating that these variables did not cause any effect on the cells.

4. Conclusions

Even though the photo-Fenton process did not completely reduce the cell density of *Microcystis aeruginosa*, the cells were

inactivated within 45 minutes of treatment. MC-LR was degraded below the detection limit of the LC method at medium and high concentrations of Fe^{2+} and H_2O_2, indicating that the oxidation process also occurred at the intracellular level. Regarding the process extrapolation to conventional water treatment plants, the milder conditions (0.6 mg L^{-1} of Fe^{2+} and 10 mg L^{-1} of H_2O_2) showed relevant results since it was possible to inactivate the cells and stop their growth without releasing toxins. This iron concentration can be easily found naturally in aquatic environments, which makes the process easier to operate, less resource-consuming, and more environmentally and economically viable.

To our knowledge, this is the first report of photo-Fenton process application aimed at *M. aeruginosa* inactivation and MC degradation, and these preliminary results demonstrated the potential of the oxidative process. However, a comprehensive and systematic approach of the process on larger scales should be conducted to confirm if its application for cyanobacterial control is worthwhile, especially with regard to the possible side effects on the aquatic ecosystem (since it is a non-selective process) and its operational viability in water treatment plants.

Conflicts of interest

There are no conflicts to declare.

Acknowledgements

The authors acknowledge the financial support provided by the Conselho Nacional de Desenvolvimento Científico e Tecnológico – CNPq (process 472233/2013-0) and Professor Armando Augusto H. Vieira for the *Microcystis aeruginosa* strain. We also thank the Multiuser Material Characterization Center (CMCM), Environmental Analysis and Equipment Laboratory (LAMEAA) and Multi-User Chemical Analysis Laboratory (LAMAQ) – UTFPR – for SEM, spectrophotometric and chromatographic analyses. Torres and Micheletto acknowledge their master's scholarship provided by the Coordenação de Aperfeiçoamento de Pessoal de Nível Superior (CAPES). The detailed review and helpful comments by anonymous reviewers are highly appreciated.

References

1 B. A. Whitton, *Ecology of Cyanobacteria II - Their Diversity in Space and Time*, Springer, New York, 1st edn, 2017.
2 J. Huisman, G. A. Codd, H. W. Paerl, B. W. Ibelings, J. M. H. Verspagen and P. M. Visser, Cyanobacterial blooms, *Nat. Rev. Microbiol.*, 2018, **16**, 471–483.
3 H. W. Paerl and J. Huisman, Climate: Blooms like it hot, *Science*, 2008, **320**, 57–58.
4 E. M. L. Janssen, Cyanobacterial peptides beyond microcystins – A review on co-occurrence, toxicity, and challenges for risk assessment, *Water Res.*, 2019, **151**, 488–499.
5 I. S. Huang and P. V. Zimba, Cyanobacterial bioactive metabolites—A review of their chemistry and biology, *Harmful Algae*, 2019, **83**, 42–94.
6 L. Šejnohová and B. Maršálek, Handbook of Cyanobacterial Monitoring and Cyanotoxin Analysis, in *Ecology of Cyanobacteria II - Their Diversity in Space and Time*, ed. B. A. Whitton, New York, 1st edn, 2017.
7 J. Meriluoto, L. Spoof and G. A. Codd, *Handbook of cyanobacterial monitoring and cyanotoxin analysis*, John Wiley & Sons, *West Sussex - UK*, 2018, vol. 410.
8 World Health Organization, *Guidelines for drinking-water quality: fourth edition incorporating the first addendum*, Geneva, 4th edn, 2017.
9 C. J. Pestana, P. J. Reeve, E. Sawade, C. F. Voldoire, K. Newton, R. Praptiwi, L. Collingnon, J. Dreyfus, P. Hobson, V. Gaget and G. Newcombe, Fate of cyanobacteria in drinking water treatment plant lagoon supernatant and sludge, *Sci. Total Environ.*, 2016, **565**, 1192–1200.
10 Environmental Protection Agency - Office of Water, *Cyanobacteria and Cyanotoxins: Information for Drinking Water Systems*, Washington DC, 2014.
11 X. He, Y. L. Liu, A. Conklin, J. Westrick, L. K. Weavers, D. D. Dionysiou, J. J. Lenhart, P. J. Mouser, D. Szlag and H. W. Walker, Toxic cyanobacteria and drinking water: Impacts, detection, and treatment, *Harmful Algae*, 2016, **54**, 174–193.
12 J. A. Westrick, D. C. Szlag, B. J. Southwell and J. Sinclair, A review of cyanobacteria and cyanotoxins removal/inactivation in drinking water treatment, *Anal. Bioanal. Chem.*, 2010, **397**, 1705–1714.
13 L. Clarizia, D. Russo, I. Di Somma, R. Marotta and R. Andreozzi, Homogeneous photo-Fenton processes at near neutral pH: A review, *Appl. Catal., B*, 2017, **209**, 358–371.
14 L. X. Pinho, J. Azevedo, Â. Brito, A. Santos, P. Tamagnini, V. J. P. Vilar, V. M. Vasconcelos and R. A. R. Boaventura, Effect of TiO_2 photocatalysis on the destruction of *Microcystis aeruginosa* cells and degradation of cyanotoxins microcystin-LR and cylindrospermopsin, *Chem. Eng. J.*, 2015, **268**, 144–152.
15 Y. Jin, S. Zhang, H. Xu, C. Ma, J. Sun, H. Li and H. Pei, Application of N-TiO_2 for visible-light photocatalytic degradation of *Cylindrospermopsis raciborskii*—More difficult than that for photodegradation of *Microcystis aeruginosa*?, *Environ. Pollut.*, 2019, **245**, 642–650.
16 J. An, N. Li, S. Wang, C. Liao, L. Zhou, T. Li, X. Wang and Y. Feng, A novel electro-coagulation-Fenton for energy efficient cyanobacteria and cyanotoxins removal without chemical addition, *J. Hazard. Mater.*, 2019, **365**, 650–658.
17 J. Sun, L. Bu, L. Deng, Z. Shi and S. Zhou, Removal of *Microcystis aeruginosa* by UV/chlorine process: Inactivation mechanism and microcystins degradation, *Chem. Eng. J.*, 2018, **349**, 408–415.
18 C. W. Chang, X. Huo and T. F. Lin, Exposure of *Microcystis aeruginosa* to hydrogen peroxide and titanium dioxide under visible light conditions: Modeling the impact of hydrogen peroxide and hydroxyl radical on cell rupture

and microcystin degradation, *Water Res.*, 2018, **141**, 217–226.
19 P. Jia, Y. Zhou, X. Zhang, Y. Zhang and R. Dai, Cyanobacterium removal and control of algal organic matter (AOM) release by UV/H_2O_2 pre-oxidation enhanced Fe(II) coagulation, *Water Res.*, 2018, **131**, 122–130.
20 X. Wu, J. Liu and J. J. Zhu, Sono-Fenton hybrid process on the inactivation of *Microcystis aeruginosa*: Extracellular and intracellular oxidation, *Ultrason. Sonochem.*, 2019, **53**, 68–76.
21 E. Ortega-gómez, M. M. B. Martín and B. E. García, Solar photo-Fenton for water disinfection: An investigation of the competitive role of model organic matter for oxidative species, *Appl. Catal., B*, 2014, **149**, 484–489.
22 E. Ortega-Gómez, M. M. B. Martín, B. E. García, J. A. S. Pérez and P. F. Ibáñez, Wastewater disinfection by neutral pH photo-Fenton: The role of solar radiation intensity, *Appl. Catal., B*, 2016, **181**, 1–6.
23 M. I. Polo-lópez, I. García-fernández, T. Velegraki, A. Katsoni, I. Oller, D. Mantzavinos and P. Fernández-Ibáñez, Mild solar photo-Fenton: An effective tool for the removal of *Fusarium* from simulated municipal effluents, *Appl. Catal., B*, 2012, **112**, 545–554.
24 D. Spuhler and J. Andre, The effect of Fe^{2+}, Fe^{3+}, H_2O_2 and the photo-Fenton reagent at near neutral pH on the solar disinfection (SODIS) at low temperatures of water containing *Escherichia coli*, K12, *Appl. Catal., B*, 2010, **96**, 126–141.
25 M. J. Abeledo-Lameiro, M. I. Polo-López, E. Ares-Mazás and H. Gómez-Couso, Inactivation of the waterborne pathogen *Cryptosporidium parvum* by photo-Fenton process under natural solar conditions, *Appl. Catal., B*, 2019, **253**, 341–347.
26 I. García-Fernández, S. Miralles-Cuevas, I. Oller, P. Fernández-Ibáñez and M. I. Polo-López, Inactivation of *E. coli*, and *E. faecalis* by solar photo-Fenton with EDDS complex at neutral pH in municipal wastewater effluents, *J. Hazard. Mater.*, 2019, **372**, 85–93.
27 S. Giannakis, M. Voumard, S. Rtimi and C. Pulgarin, Bacterial disinfection by the photo-Fenton process: Extracellular oxidation or intracellular photo-catalysis?, *Appl. Catal., B*, 2018, **227**, 285–295.
28 P. R. Gorham, J. McLachlan, U. T. Hammer and W. K. Kim, Isolation and culture of toxic strains of *Anabaena flos-aquae* (Lyngb.) de Bréb, *SIL Proceedings, 1922–2010: Internationale Vereinigung für Theoretische und Angewandte Limnologie: Verhandlungen (1922–2010)*, 1964, **15**, 796–804.
29 SYLVANIA, Frequently Asked Questions, https://s3-us-west-2.amazonaws.com/oww-files-public/e/e8/Conversion_lux.pdf. (accessed February 2020).
30 M. A. Torres, M. V. De Liz, L. R. R. Martins and A. M. Freitas, Does the photo-Fenton reaction work for microalgae control? A case study with *Desmodesmus subspicatus*, *Photochem. Photobiol. Sci.*, 2018, **17**, 517–521.
31 E. Ortega-Gómez, B. E. García, M. M. B. Martín, P. F. Ibáñez and J. A. S. Pérez, Inactivation of natural enteric bacteria in real municipal wastewater by solar photo-Fenton at neutral pH, *Water Res.*, 2014, **63**, 316–324.
32 R. Schick, I. Strasser and H.-H. Stabel, Fluorometric determination of low concentrations of H_2O_2 in water: Comparison with two other methods and application to environmental samples and drinking-water treatment, *Water Res.*, 1997, **31**, 1371–1378.
33 APHA-AWWA-WEF, *Standard Methods for the Examination of Water and Wastewater*, American Public Health Association, Washington DC, 2012.
34 International council for harmonization of technical requirements for pharmaceuticals for human use, Bioanalytical Method Validation M10 guideline, https://www.ich.org/products/guidelines/multidisciplinary/article/multidisciplinary-guidelines.html (accessed December 2019).
35 S. Giannakis, M. I. Polo López, D. Spuhler, J. A. Sánchez Pérez, P. Fernández Ibáñez and C. Pulgarin, Solar disinfection is an augmentable, *in situ*-generated photo-Fenton reaction—Part 1: A review of the mechanisms and the fundamental aspects of the process, *Appl. Catal., B*, 2016, **199**, 199–223.
36 J. Wang, Z. Chen, H. Chen and Y. Wen, Effect of hydrogen peroxide on *Microcystic aeruginosa*: Role of cytochromes P450, *Sci. Total Environ.*, 2018, **626**, 211–218.
37 A. Latifi, M. Ruiz and C. C. Zhang, Oxidative stress in cyanobacteria, *FEMS Microbiol. Rev.*, 2009, **33**, 258–278.
38 E. Ortega-Gómez, B. E. García, M. M. B. Martín and J. A. S. Pérez, Inactivation of *Enterococcus faecalis* in simulated wastewater treatment plant effluent by solar photo-Fenton at initial neutral pH, *Catal. Today*, 2013, **209**, 195–200.
39 P. A. Soares, M. Batalha, S. M. A. Guelli, U. Souza, R. A. R. Boaventura and V. J. P. Vilar, Enhancement of a solar photo-Fenton reaction with ferric-organic ligands for the treatment of acrylic-textile dyeing wastewater, *J. Environ. Manage.*, 2015, **152**, 120–131.